Advances in Nano Research, *Vol. 15, No. 2 (2023) 175-189*
https://doi.org/10.12989/anr.2023.15.2.175

Elastic buckling performance of FG porous plates embedded between CNTRC piezoelectric patches based on a novel quasi 3D-HSDT in hygrothermal environment

Yujie Zhang[1], Zhihang Guo[1], Yimin Gong[1], Jianzhong Shi[**1],
Mohamed Hechmi El Ouni[2] and Farhan Alhosny[*3]

[1]*School of Environmental Engineering, Wuhan Textile University, Wuhan, Hubei, 430200, China*
[2]*Department of Civil Engineering, College of Engineering, King Khalid University, Abha, Saudi Arabia*
[3]*Mechanical Engineering Department, UAE University, UAE*

(*Received March 3, 2023, Revised May 14, 2023, Accepted June 8, 2023*)

Abstract. The under-evaluation structure includes a functionally graded porous (FGP) core which is confined by two piezoelectric carbon nanotubes reinforced composite (CNTRC) layers. The whole structure rests on the Pasternak foundation. Using quasi-3D hyperbolic shear deformation theory, governing equations of a sandwich plate are driven. Moreover, face sheets are subjected to the electric field and the whole model is under thermal loading. The properties of all layers alter continuously along with thickness direction due to the CNTs and pores distributions. By conducting the current study, the results emerged in detail to assess the effects of different parameters on buckling of structure. As instance, it is revealed that highest and lowest critical buckling load and consequently stiffness, is due to the *V-A* and *A-V* CNTs dispersion type, respectively. Furthermore, it is revealed that by porosity coefficient enhancement, critical buckling load and consequently, stiffness reduces dramatically. Current paper results can be used in various high-tech industries as aerospace factories.

Keywords: buckling analysis; CNTs reinforced composite; piezoelectricity; quasi 3D hyperbolic shear deformation theory; sandwich plates

1. Introduction

The new generation of electronic devices development in addition to the industries demands that address mentioned devices to tolerate different electro-thermo-mechanical conditions, generate a great engineering challenge regarding their design and their manufacturing (Esfandiari *et al*. 2023, Farhangi *et al*. 2023, Izadifar *et al*. 2021, 2023, Khoei *et al*. 2022, Kianezhad *et al*. 2022, 2023, Torabipour *et al*. 2023, Ikbarieh *et al*. 2023, Mehrdad *et al*. 2013). An inevitable member of the electronic devices' family is piezoelectric structures which play an essential role in various applications of different devices. Therefore, scientists should understand the mechanical behavior of different piezoelectric structures deeply to increase the efficiency of different electrical and mechanical devices (Ghorbanpour Arani *et al*. 2021, Arshid *et al*. 2023b, Vosoughkhosravi *et al*. 2022).

Based on the piezoelectricity effect some materials produce electrical potential under mechanical deformation. The electromechanical coupling in this kind of material can be hired to handle some important applications (Amir *et al*. 2020a, Vosoughkhosravi and Jafari, 2022a, b, Arshid *et al*. 2022, Khoddami Maraghi *et al*. 2022). Also, advanced composites are Functionally Graded Materials (FGMs) based layers that undergoes continuous mechanical properties' variation. The concept of FGMs, firstly, proposed in 1984 by materials scholars in the Sendai area. They used FGMs to fabricate barriers against thermal wastage (Koizumi, 1997). In 1998, Reddy and Chin (1998), studied the thermoelastic behavior of FG plates. They didn't limit their work to plates and also, put FG cylinders under examination. Han *et al*. (2001) used Fourier transform techniques to study stress waves in FG plates. For this reason, they put their model under incident pressure wave. In another work, they had an evaluation on the FGMs' wave propagating behavior by the means of another numerical method (Han *et al*. 2000). Najafizadeh and Eslami (2002), evaluated FG circular plates' buckling behavior. Their model was loaded radially. After that, research conducted by Vel *et al*. (2004) to obtain three-dimensional (3D) deformation pattern of a simply supported rectangular FG plates. Their model was under various loads. Moreover, using classical plate theory (CPT), Javaheri and Eslami (2002) succeed to handle thermal equations of a FGM plate. They concluded critical buckling temperature has a directional relationship with dimension ratio *b*/*a* of FG plates. Beside this, 3D thermal buckling behavior of FGMs is evaluated by Na and Kim (2003). They examined the effects of the different geometric parameters and various volume fraction distributions on critical buckling temperature. Nonlinear static and dynamic stability of FG

*Corresponding author, Ph.D.,
E-mail: Farhanalhosny@gmail.com
**Co-corresponding author, Professor,
E-mail: SHI4954@126.com

Copyright © 2023 Techno-Press, Ltd.

ISSN: 2287-237X (Print), 2287-2388 (Online)

plates and shells conducted by Duc (2014). In the passage of years, the applications of FGM become more broaden and this wide range of applications showed need to more accurate plate theories like higher-order shear deformation plate theory (HSDT) or first-order shear deformation plate theory (FSDT) (Alhaifi *et al*. 2021, Soleimani-Javid *et al*. 2021a, Wang *et al*. 2021). One of the previous works backs to 2004, when Yang *et al*. (2004) conducted a study about dynamic stability behavior of rectangular FGM plates. Their study was based on uniform temperature variation condition. As another paper, Efraim and Eisenberger (2007) used FSDT in order to have deep research on thickness effect on vibrational behavior of FGM plates. Shen (2009) studied post-buckling in thermal environments for an FG plate reinforced by Piezoelectric Fiber composite. Their model was simply supported. Beside this, a quasi-3D hyperbolic shear deformation plate theory (QHSDT) is hired by Benahmed *et al*. (2017) to address the mechanical behavior of FG plates. Moreover, Shahsavari *et al*. (2018) assuming a porous FG plate as model and by the means of QHSDT provided a free vibration analysis for such models. Dynamic instability of sandwich beams made of isotropic core and FG graphene platelets-reinforced composite face sheets considered by Asgari *et al*. (2022). Cong *et al*. (2018) considered nonlinear thermo-mechanical buckling and post-buckling response of porous FGM plates using Reddy's theory. Free vibration analysis of FG porous joined truncated conical-cylindrical shell reinforced by graphene platelets provided by Kiarasi *et al*. (2021). Also, Duc *et al*. (2018) provided nonlinear dynamic response of FGM porous plates on elastic foundation subjected to thermal and mechanical loads using the FSDT. Moreover, analytical solutions for nonlinear vibration of porous FG sandwich plate subjected to blast loading provided by Quan *et al*. (2022). In another work (Babaei *et al*. 2022a) transient thermal stresses in FG porous rotating truncated cones was investigated. Dynamic analysis of FG carbon nanotube reinforced composite beam resting on viscoelastic foundation was investigated by Kiarasi *et al*. (2022). Other similar works can also be found in the available literature (Alhaifi *et al*. 2023, Arshid *et al*. 2023a, 2021a, Soleimani-Javid *et al*. 2021b). There are also novel approaches based purely on deep neural network (DNN). They totally avoid a classical discretization, are extremely efficient, automatically account for uncertainties and are a natural framework for inverse analysis and optimization. In this field, an energy approach to the solution of partial differential equations in computational mechanics via machine learning was presented by Samaniego *et al*. (2020). Also, deep autoencoder based energy method for the bending, vibration, and buckling analysis of Kirchhoff plates with transfer learning was studied by Zhuang *et al*. (2021). A deep collocation method for the bending analysis of Kirchhoff plate was conducted by Guo *et al*. (2019). Recently, curved flexoelectric and piezoelectric micro-beams for nonlinear vibration analysis of energy harvesting was studied by Thai *et al*. (2023). Rabczuk *et al*. (2023) investigated nonlocal strong forms of thin plate, gradient elasticity, magneto-electro-elasticity and phase field fracture by nonlocal operator method.

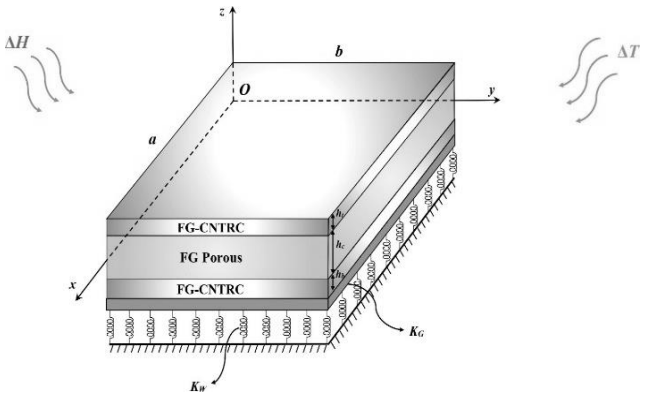

Fig. 1 Schematic diagram of the under-consideration model under hygrothermal environment

Motivated by previous attempts, this paper aims to improve the knowledge of sandwich plates and examine the mechanical buckling behavior in hygrothermal environment. In order to obtain results more touchable and closer to the fact and experimental studies, novel QHSDT is hired to represent different arbitrary points in structure. Mathematical solutions are gained for sandwich plate, and results' reliability is verified by providing a comparison among the gained results from current study and those in previous researches. The governing equations are derived and solved by using virtual displacement principle and the results seem to be useful in aerospace, automotive, civil, and mechanical engineering.

2. Sandwich plate modelling

This section focuses on introducing current model which is under examination. Fig. 1 shows a rectangular sandwich plate including a FGP core compressed by piezoelectric composite faces with geometrical components as it is visible in figure. Whole structure assumed to be placed on the Pasternak elastic foundation. Also, h_c, h_t, and h_b represent thickness of porous core, top face sheet and bottom face sheet, respectively, where the total thickness is $h=h_t+h_c+h_b$. The coordinate system assumed to be cartesian (x, y, z) as it is visible in the Fig. 1. Moreover, the geometrical properties of the model include length a, width b and height h. Also, Face sheets assume to be subjected to electric fields. Also, it is assumed that all three layers are fully bonded to each other. In order to make analyzation understanding simpler, in this paper, it is decided to present different relations and equations in two divided portions (FGP core and composite piezoelectric face sheets). At the end of each section, strain energy of each part is obtained using QHSDT. By adding the energy of different parts together, the total strain energy of aforementioned structure emerges mathematically.

In order to increase accuracy, in this research, QHSDT is used to express displacement field of sandwich model. According to this theory, the displacements of an arbitrary point neither in porous core nor in composite faces can be presented as (Arshid *et al*. 2020c):

$$\begin{matrix}\tilde{w}(x,y,z)=\varphi(x,y)g(z)+w_s(x,y)+w_b(x,y)\\ \tilde{v}(x,y,z)=-w_{s,y}(x,y)f(z)-w_{b,y}(x,y)z+v(x,y)\\ \tilde{u}(x,y,z)=-w_{s,x}(x,y)f(z)-w_{b,x}(x,y)z+u(x,y)\end{matrix} \quad (1)$$

where u, v, w_b and w_s are the displacement representatives in the x direction, y direction, transverse displacement due to the bending effect along with z direction and transverse displacement due to the shear impact along with z direction, respectively. It is noteworthy mentioning that, subscript ,i $(i=x,y,z)$ serves as derivative respect to i. Also, φ serves as normal stress effect parameter and basically it is an additional. $g(z)$ and $f(z)$ are representative of:

$$f(z)=\left\{\frac{-z+(\frac{h}{\pi})\,sinh(\frac{\pi z}{h})}{-1+cosh(\frac{\pi}{2})}\right\}, \quad (2)$$

$$g(z)=\{1-f_{,z}(z)\} \quad (3)$$

Hiring von-Karman's assumptions, using mentioned displacement field, and neglecting nonlinearity, strain field can be defined as (Berghouti *et al*. 2019, Khorasani *et al*. 2021b):

$$\varepsilon_{xx}=\frac{\partial\tilde{u}}{\partial x},\qquad \varepsilon_{yy}=\frac{\partial\tilde{v}}{\partial y},$$

$$\varepsilon_{zz}=\frac{\partial\tilde{w}}{\partial z},\qquad \varepsilon_{xy}=\frac{1}{2}\left(\frac{\partial\tilde{u}}{\partial y}+\frac{\partial\tilde{v}}{\partial x}\right), \quad (4)$$

$$\varepsilon_{xz}=\frac{1}{2}g(z)\left(\frac{\partial\varphi}{\partial x}+\frac{\partial w_s}{\partial x}\right),\ \ \varepsilon_{yz}=\frac{1}{2}g(z)\left(\frac{\partial\varphi}{\partial y}+\frac{\partial w_s}{\partial y}\right)$$

2.1 FGP Core

SUS304 used as material for core construction. As mentioned in previous section, a porous layer is used as core portion of abovementioned sandwich plate. In this section, the stress-strain relations of the core are derived as follows (Arshid *et al*. 2020b, Ebrahimi 2019, Singh and Azam 2021):

$$\begin{bmatrix}{\sigma_{xx}}^c\\ {\sigma_{yy}}^c\\ {\sigma_{zz}}^c\\ {\sigma_{xy}}^c\\ {\sigma_{yz}}^c\\ {\sigma_{xz}}^c\end{bmatrix}=\begin{bmatrix}C_{11}&C_{12}&C_{13}&0&0&0\\ C_{12}&C_{22}&C_{23}&0&0&0\\ C_{13}&C_{23}&C_{33}&0&0&0\\ 0&0&0&C_{44}&0&0\\ 0&0&0&0&C_{55}&0\\ 0&0&0&0&0&C_{66}\end{bmatrix}\begin{bmatrix}\varepsilon_{xx}-\alpha_{11}\Delta T-\beta_{11}\Delta H\\ \varepsilon_{yy}-\alpha_{22}\Delta T-\beta_{22}\Delta H\\ \varepsilon_{zz}-\alpha_{33}\Delta T-\beta_{33}\Delta H\\ 2\varepsilon_{xy}\\ 2\varepsilon_{yz}\\ 2\varepsilon_{xz}\end{bmatrix} \quad (5)$$

where, C, α, ΔT and superscript c represent elastic factor, thermal index, temperature variation and porous core, respectively. Moreover, β and ΔH are moisture constant and humidity difference. Elastic factors assumed as (Arshid *et al*. 2020a):

$$C_{11}=C_{22}=C_{33}=(1-v)\frac{E_c(z)}{(1-2v)(1+v)},$$

$$C_{44}=C_{55}=C_{66}=G(z)=\frac{E_c(z)}{2(1+v)}, \quad (6)$$

$$C_{12}=C_{13}=C_{23}=\frac{vE_c(z)}{(1-2v)(1+v)}$$

in which $E_c(z)$, $G(z)$ and v indicate elastic modulus, shear modulus and Poisson's ratio, respectively.

Porosity distribution type within core plate affects elastic constants by alternation in elastic modulus and core density. There are three well-known different type of porosity distribution, uniform, uneven and even. Porosity distribution named even addresses pores distribution symmetrically through porous layer and elastic modulus and density distribution assume to be (Arshid *et al*. 2019a):

$$E_c(z)=E_0\left[1-e_1\,cos(\frac{\pi z}{h_c})\right] \quad (7)$$

$$\rho_c(z)=\rho_0\left[1-e_m\,cos(\frac{\pi z}{h_c})\right], \quad (8)$$

$$e_m=1-\sqrt{1-e_1}, \quad (9)$$

where, e_1 is the porosity coefficient. Also, e_m is mass density factor. On the other hand, if porosity distribution be uneven type so (Arshid and Amir 2021, Dat *et al*. 2022):

$$E_c(z)=E_0\left[1-e_1\,cos(\left\{\frac{\pi}{2h_c}(z+\frac{h_c}{2})\right\})\right] \quad (10)$$

$$\rho_c(z)=\rho_0\left[1-e_m\,cos(\left\{\frac{\pi}{2h_c}(z+\frac{h_c}{2})\right\})\right], \quad (11)$$

And finally, thickness parameter independency is visible at modulus and density equations in the case of uniform porosity distribution as (Babaei *et al*. 2020, 2022b):

$$E_c(z)=E_0[1-e_1\zeta], \quad (12)$$

$$\rho_c(z)=\rho_0\sqrt{1-e_1\zeta}, \quad (13)$$

$$\zeta=\frac{1}{e_1}-\frac{1}{e_1}(\frac{2}{\pi}\sqrt{1-e_1}-\frac{2}{\pi}+1)^2 \quad (14)$$

Finally, using abovementioned equations, the strain energy of FGP core is derived as (Khorasani, Soleimani-Javid, *et al*. 2020, Mousavi *et al*. 2021):

$$\cup^c=\int_V\frac{1}{2}\begin{bmatrix}{\sigma_{xx}}^c\varepsilon_{xx}+{\sigma_{yy}}^c\varepsilon_{yy}+{\sigma_{zz}}^c\varepsilon_{zz}\\ +2{\sigma_{xy}}^c\varepsilon_{xy}+2{\sigma_{xz}}^c\varepsilon_{xz}+2{\sigma_{yz}}^c\varepsilon_{yz}\end{bmatrix}d\forall \quad (15)$$

2.2 Piezoelectric nanocomposite face sheets

Nanocomposite face sheets are made of polymer matrix and CNT fibers as reinforcing phase. To gain governing equations of sandwich model, the stress-strain relationship of piezoelectric composite face sheets should be presented.

Therefore, inspired of previous studies, stress field for piezoelectric composite layers can be determined as follows (Amir *et al*. 2018, Chan *et al*. 2020):

$$\begin{bmatrix}\sigma_{xx}{}^{f}\\ \sigma_{yy}{}^{f}\\ \sigma_{zz}{}^{f}\\ \sigma_{xy}{}^{f}\\ \sigma_{yz}{}^{f}\\ \sigma_{xz}{}^{f}\end{bmatrix}=\begin{bmatrix}Q_{11} & Q_{12} & Q_{13} & 0 & 0 & 0\\ Q_{12} & Q_{22} & Q_{23} & 0 & 0 & 0\\ Q_{13} & Q_{23} & Q_{33} & 0 & 0 & 0\\ 0 & 0 & 0 & Q_{44} & 0 & 0\\ 0 & 0 & 0 & 0 & Q_{55} & 0\\ 0 & 0 & 0 & 0 & 0 & Q_{66}\end{bmatrix}\begin{bmatrix}\varepsilon_{xx}-\alpha_{11}\Delta T-\beta_{11}\Delta H\\ \varepsilon_{yy}-\alpha_{22}\Delta T-\beta_{22}\Delta H\\ \varepsilon_{zz}-\alpha_{33}\Delta T-\beta_{33}\Delta H\\ 2\varepsilon_{xy}\\ 2\varepsilon_{yz}\\ 2\varepsilon_{xz}\end{bmatrix} \quad (16)$$
$$-\begin{bmatrix}0 & 0 & e_{31}\\ 0 & 0 & e_{32}\\ 0 & 0 & e_{33}\\ 0 & 0 & 0\\ 0 & e_{24} & 0\\ e_{15} & 0 & 0\end{bmatrix}\begin{bmatrix}E_x\\ E_y\\ E_z\end{bmatrix},$$

where, *E*, *f*, *Q* and *e* are electrical field, first syllable of the word "faces", elastic and piezoelectric constants representatives. Moreover, the electrical potential and fields can be defined as (Kargar *et al*. 2021):

$$\overline{\phi}(x,y,z,t)=-\phi(x,y,t)\,cos(\frac{\pi z}{h_f})+\frac{2\phi_0}{h_f}z \quad (17)$$

$$E_x=-\overline{\phi}_{,x},\qquad E_y=-\overline{\phi}_{,y},\qquad E_z=-\overline{\phi}_{,z} \quad (18)$$

where, ϕ_0 denotes external voltage which is applied on faces. Furthermore, elastic factors are defined as (Arshid and Khorshidvand 2018):

$$Q_{11}=\frac{E_{11}}{\Theta}(1-v_{32}v_{23}),\qquad Q_{22}=\frac{E_{22}}{\Theta}(1-v_{31}v_{13}),$$

$$Q_{32}=Q_{23}=\frac{E_{22}}{\Theta}(v_{32}+v_{12}v_{31}),\qquad Q_{12}=Q_{21}=\frac{E_{11}}{\Theta}(v_{21}+v_{31}v_{23}),$$
$$Q_{33}=\frac{E_{33}}{\Theta}(1-v_{12}v_{21}),\qquad Q_{13}=Q_{31}=\frac{E_{11}}{\Theta}(v_{31}+v_{21}v_{32}), \quad (19)$$

$$Q_{44}=Q_{55}=Q_{66}=G_{12}=G_{13}=G_{23},$$

where, E_{ij} and v indicate elastic moduli and Poisson's ratio and:

$$\Theta=1-v_{21}v_{12}-v_{32}v_{23}-v_{13}v_{31}-2v_{13}v_{32}v_{12},$$

$$E_{33}=E_{22},\qquad E_{33}=E_{22},$$
$$v_{13}=v_{12},\qquad v_{13}=v_{12}, \quad (20)$$

As it is clear, knowing mechanical properties of composite layer is essential to derive and solve governing equations mathematically. For this aim, extended rule of mixture (ERM) is hired to mix mechanical properties of matrix and reinforcing phases and introduce mechanical properties of whole composite layer (Anh *et al*. 2021, Dat *et al*. 2021, Wu *et al*. 2020).

Based on ERM, the material properties of composite faces are (Arshid *et al*. 2019b):

$$v_{12}=V_{main}^{CNT}v_{12}^{CNT}+V^{P}v^{P}, \quad (21)$$

$$\rho_c=V^{CNT}\rho^{CNT}+V^{P}\rho^{P}, \quad (22)$$

$$E_{11}=\eta_1V^{CNT}E_{11}^{CNT}+V^{P}E^{P}, \quad (23)$$

$$\alpha_{11}=V^{CNT}\alpha_{11}{}^{CNT}+V^{P}\alpha^{P}, \quad (24)$$

$$\alpha_{22}=\alpha_{33}=(1+v_{12}^{CNT})V^{CNT}\alpha_{22}{}^{CNT}+(1+v^{P})V^{P}\alpha^{P}-v_{12}\alpha_{11} \quad (25)$$

$$\frac{\eta_3}{G_{12}}=\frac{V^{CNT}}{G_{12}^{CNT}}+\frac{V^{P}}{G^{P}},\qquad \frac{\eta_2}{E_{22}}=\frac{V^{CNT}}{E_{22}^{CNT}}+\frac{V^{P}}{E^{P}} \quad (26)$$

where letter *P* reminds polymeric matrix and η_k (k = 1,2, 3) is the CNTs efficiency parameter which has dependency to total CNTs volume which is existed in composite, as mentioned in Table 1 (Arshid *et al*. 2021b, Mehar and Panda 2017).

V^{P} and V^{CNT} are volume fraction for matrix and volume fraction for CNTs, and their summation should be equal to 1 (Fattahi *et al*. 2019). It should be noted that V^{CNT} is different from $V^{CNT}{}_{\text{main}}$ which addressed uniform dispersion pattern of CNTs through polymer matrix phase. As another expression, V^{CNT} is *CNT*s dispersion pattern dependent. V^{CNT} and $V^{CNT}{}_{\text{main}}$ can be presented as (Amir *et al*. 2019, Arshid *et al*. 2021c):

$$V_{main}^{CNT}=\frac{w^{CNT}}{w^{CNT}+(\frac{\rho^{CNT}}{\rho^{P}})-(\frac{\rho^{CNT}}{\rho^{P}})w^{CNT}} \quad (27)$$

$$V_i^{CNT}=\begin{cases}V_{main}^{CNT} & U-U\\ \left[1-\frac{2}{h_i}(z\pm\frac{h_c+h_i}{2})\right]V_{main}^{CNT} & FGA-V\\ \left[1+\frac{2}{h_i}(z\pm\frac{h_c+h_i}{2})\right]V_{main}^{CNT} & FGV-A\\ 2\left[1-\frac{2}{h_i}(z\pm\frac{h_c+h_i}{2})\right]V_{main}^{CNT} & FGO-O\\ \left[\frac{4}{h_i}(\left|z\pm\frac{h_c+h_i}{2}\right|)\right]V_{main}^{CNT} & FGX-X\end{cases}_{i=t,b} \quad (28)$$

In abovementioned equations, subscript *c*, *t* and *b* are abbreviation of words Core, Top and Bottom face sheets, one after another. Beside this, *w* is mass fraction, *FG A-V*, *FG V-A*, *FG O-O* and *FG X-X* denote CNTs dispersion pattern in matrix phase and *U-U* is representative of uniform dispersion pattern.

At the end, using abovementioned relations, the strain energy of piezoelectric composite face sheets is presented as (Arshid *et al*. 2019c):

$$\cup^{f}=\frac{1}{2}\int_V\begin{pmatrix}\sigma_{xx}\varepsilon_{xx}+\sigma_{yy}\varepsilon_{yy}+\sigma_{zz}\varepsilon_{zz}\\ +2\sigma_{xy}\varepsilon_{xy}+2\sigma_{xz}\varepsilon_{xz}+2\sigma_{yz}\varepsilon_{yz}\\ -D_xE_x-D_yE_y-D_zE_z\end{pmatrix}d\forall \quad (29)$$

where, D_i stands for the electrical displacement and it is defined as (Mohammadimehr *et al*. 2019, Safari *et al*. 2021):

Table 1 Efficiency parameters of CNTs (Arshid *et al*. 2021b, Mehar and Panda 2017)

V_{main}^{CNT}	η_1	η_2	η_3
0.12	0.137	1.022	0.715
0.17	0.142	1.626	1.138
0.28	0.141	1.585	1.109

$$\begin{bmatrix} D_x \\ D_y \\ D_z \end{bmatrix} = \begin{bmatrix} 0 & 0 & 0 & 0 & 0 & e_{15} \\ 0 & 0 & 0 & 0 & e_{24} & 0 \\ e_{31} & e_{32} & e_{33} & 0 & 0 & 0 \end{bmatrix} \begin{bmatrix} \varepsilon_{xx} \\ \varepsilon_{yy} \\ \varepsilon_{zz} \\ 2\varepsilon_{xy} \\ 2\varepsilon_{yz} \\ 2\varepsilon_{xz} \end{bmatrix} + \begin{bmatrix} d_{11} & 0 & 0 \\ 0 & d_{22} & 0 \\ 0 & 0 & d_{33} \end{bmatrix} \begin{bmatrix} E_x \\ E_y \\ E_z \end{bmatrix} \tag{30}$$

where, *d* is dielectric constant.

3. Governing equations

The virtual displacement principle is used to obtain governing equations making use of strain, energies and external works. Mentioned principle can be presented as (Amir *et al*. 2020d, Dinh Dat *et al*. 2022):

$$\delta\Pi = \delta(U^c + U^f - \Gamma - \Lambda - \Sigma) = 0 \tag{31}$$

in which, U, Γ, Λ and Σ are strain energy, external work due to the Pasternak foundation, electrical field and thermal environment, respectively. It is worthwhile mentioning that superscripts *c* and *f* are first syllables of words core and face sheets. In this paper Pasternak foundation assumed to carry sandwich model weight. This foundation has capability to simulate transverse load in addition to normal load (Bi *et al*. 2021). The force applied on sandwich model resulted by foundation can be presented as (Amir *et al*. 2020b):

$$F_{Pasternakfoundation} = K_w[w_b + w_s] - K_g\frac{\partial^2[w_b + w_s]}{\partial x^2} - K_g\frac{\partial^2[w_b + w_s]}{\partial y^2} \tag{32}$$

where Winkler constant is presented by sign K_w and shear layer parameter is shown by K_g. So, the external work due to the Pasternak substrate is (Babaei *et al*. 2019, Arshid *et al*. 2023c):

$$\Gamma = \frac{1}{2}\int_A -F_{Pasternakfoundation}(w_b + w_s)dA \tag{33}$$

External load due to the electrical field is simulated as (Quan *et al*. 2021, 2022a):

$$N_x^E = -2e_{31}\phi_0, \qquad N_y^E = -2e_{32}\phi_0 \tag{34}$$

$$\Lambda_{Electrical} = \frac{1}{2}\int_A N_x^E\langle w_{b,x} + w_{s,x}\rangle^2\,dA + \frac{1}{2}\int_A N_y^E\langle w_{b,y} + w_{s,y}\rangle^2\,dA \tag{35}$$

The hygrothermal external work due to the hygrothermal loads in *x* and *y* directions can be determined as follows (Dat *et al*. 2020, Quang *et al*. 2021):

$$\Sigma = \frac{1}{2}\int_A N_x^{HT}\langle w_{b,x} + w_{s,x}\rangle^2\,dA + \frac{1}{2}\int_A N_y^{HT}\langle w_{b,y} + w_{s,y}\rangle^2\,dA \tag{36}$$

where hygrothermal loads due to the temperature and moisture differences in *x* and *y* direction is depicted by N_x and N_y as (Chan *et al*. 2020, Khorasani *et al*. 2020a):

$$N_x^{HT} = \int_{-h/2}^{+h/2}\left[Q_{11}^{c,f}\alpha_{11}^{c,f} + Q_{12}^{c,f}\alpha_{22}^{c,f} + Q_{13}^{c,f}\alpha_{33}^{c,f}\right]\Delta T dz + \int_{-h/2}^{+h/2}\left[Q_{11}^{c,f}\beta_{11}^{c,f} + Q_{12}^{c,f}\beta_{22}^{c,f} + Q_{13}^{c,f}\beta_{33}^{c,f}\right]\Delta H dz, \tag{37}$$

$$N_y^{HT} = \int_{-h/2}^{+h/2}\left[Q_{12}^{c,f}\alpha_{11}^{c,f} + Q_{22}^{c,f}\alpha_{22}^{c,f} + Q_{23}^{c,f}\alpha_{33}^{c,f}\right]\Delta T dz + \int_{-h/2}^{+h/2}\left[Q_{12}^{c,f}\beta_{11}^{c,f} + Q_{22}^{c,f}\beta_{22}^{c,f} + Q_{23}^{c,f}\beta_{33}^{c,f}\right]\Delta H dz, \tag{38}$$

It should be noted that the changes in plate's dimensions with temperature variations are neglected in this work due to its small amount in comparison to plate's dimensions.

On the foundation of variational approach, the governing equations are gained in terms of displacements. Therefore, the factors of δv, δw_b, δu, δw_s, $\delta\phi$ and $\delta\varphi$ should be distinct and equal to zero. So, six differential governing equations are extracted as:

δu:

$$\begin{aligned} &-Q_{110}\left(\frac{\partial^2}{\partial x^2}u\right) + Q_{111}\left(\frac{\partial^3}{\partial x^3}w_b\right) + Q_{113}\left(\frac{\partial^3}{\partial x^3}w_s\right) \\ &-Q_{120}\left(\frac{\partial^2}{\partial x\partial y}v\right) + Q_{121}\left(\frac{\partial 3}{\partial x\partial y^2}w_b\right) - Q_{136}\left(\frac{\partial}{\partial x}\varphi\right) \\ &-Q_{660}\left(\frac{\partial^2}{\partial y^2}u\right) + 2Q_{661}\left(\frac{\partial^3}{\partial x\partial y^2}w_b\right) + 2Q_{663}\left(\frac{\partial^3}{\partial x\partial y^2}w_s\right) \\ &-Q_{660}(\frac{\partial^2}{\partial x\partial y}v) - E_{310}(\frac{\partial}{\partial x}\phi) + Q_{123}(\frac{\partial^3}{\partial x\partial y^2}w_s) = 0 \end{aligned} \tag{39}$$

δv:

$$\begin{aligned} &-Q_{120}\left(\frac{\partial^2}{\partial x\partial y}u\right) + Q_{121}\left(\frac{\partial^3}{\partial x^2\partial y}w_b\right) + Q_{123}\left(\frac{\partial^3}{\partial x^2\partial y}w_s\right) \\ &-Q_{220}\left(\frac{\partial^2}{\partial y^2}v\right) - E_{320}\left(\frac{\partial}{\partial y}\phi\right) + Q_{221}\left(\frac{\partial^3}{\partial y^3}w_b\right) \\ &+Q_{223}\left(\frac{\partial^3}{\partial y^3}w_s\right) - Q_{236}\left(\frac{\partial}{\partial y}\varphi\right) + 2Q_{663}\left(\frac{\partial^3}{\partial x^2\partial y}w_s\right) \\ &-Q_{660}(\frac{\partial^2}{\partial x^2}v) - Q_{660}(\frac{\partial^2}{\partial y\partial x}u) + 2Q_{661}(\frac{\partial^3}{\partial x^2\partial y}w_b) = 0 \end{aligned} \tag{40}$$

δw_b:

$$\begin{aligned} &-Q_{121}\left(\frac{\partial^3}{\partial x\partial y^2}u\right) + 2Q_{122}\left(\frac{\partial^4}{\partial x^2\partial y^2}w_b\right) \\ &+2Q_{124}\left(\frac{\partial^4}{\partial x^2\partial y^2}w_s\right) - Q_{221}\left(\frac{\partial^3}{\partial y^3}v\right) + Q_{222}\left(\frac{\partial^4}{\partial y^4}w_b\right) \\ &+Q_{224}\left(\frac{\partial^4}{\partial y^4}w_s\right) - Q_{237}\left(\frac{\partial^2}{\partial y^2}\varphi\right) - E_{321}\left(\frac{\partial^2}{\partial y^2}\phi\right) \end{aligned} \tag{41}$$

$$-2Q_{661}\left(\frac{\partial^3}{\partial x^2\partial y}v\right)-Q_{137}\left(\frac{\partial^4}{\partial x^2}\varphi\right)+4Q_{662}\left(\frac{\partial^4}{\partial x^2\partial y^2}w_b\right)$$
$$+4Q_{664}\left(\frac{\partial^4}{\partial x^2\partial y^2}w_s\right)-2Q_{661}\left(\frac{\partial^3}{\partial y^2\partial x}u\right)-Q_{111}\left(\frac{\partial^3}{\partial x^3}u\right)$$
$$+Q_{112}\left(\frac{\partial^4}{\partial x^4}w_b\right)+Q_{114}\left(\frac{\partial^4}{\partial x^4}w_s\right)-Q_{121}\left(\frac{\partial^3}{\partial x^2\partial y}v\right)$$
$$-E_{311}(\frac{\partial^4}{\partial x^2}\phi)=0$$

δw_s:

$$Q_{114}\left(\frac{\partial^4}{\partial x^4}w_b\right)+2Q_{125}\left(\frac{\partial^4}{\partial x^2\partial y^2}w_s\right)+E_{1510}\left(\frac{\partial^2}{\partial x^2}\phi\right)$$
$$-Q_{113}\left(\frac{\partial^3}{\partial x^3}u\right)-2Q_{663}\left(\frac{\partial^3}{\partial x^2\partial y}v\right)-Q_{123}\left(\frac{\partial^3}{\partial x^2\partial y}v\right)$$
$$-E_{132}\left(\frac{\partial^2}{\partial x^2}\varphi\right)-Q_{138}\left(\frac{\partial^2}{\partial x^2}\varphi\right)-Q_{123}\left(\frac{\partial^3}{\partial y^2\partial x}u\right)$$
$$+Q_{115}\left(\frac{\partial^4}{\partial x^4}w_s\right)+E_{2410}\left(\frac{\partial^2}{\partial y^2}\phi\right)-E_{323}\left(\frac{\partial^2}{\partial y^2}\phi\right)$$
$$-Q_{223}\left(\frac{\partial^3}{\partial y^3}v\right)+Q_{224}\left(\frac{\partial^4}{\partial y^4}w_b\right)+Q_{225}\left(\frac{\partial^4}{\partial y^4}w_s\right)$$
$$-E_{232}\left(\frac{\partial^2}{\partial y^2}\varphi\right)-2Q_{663}\left(\frac{\partial^3}{\partial x\partial y^2}u\right)-Q_{4410}\left(\frac{\partial^2}{\partial y^2}w_s\right)$$
$$-Q_{238}\left(\frac{\partial^2}{\partial y^2}\varphi\right)-Q_{4410}\left(\frac{\partial^2}{\partial y^2}\phi\right)+4Q_{664}\left(\frac{\partial^4}{\partial x^2\partial y^2}w_b\right)$$
$$-Q_{5510}\left(\frac{\partial^2}{\partial x^2}w_s\right)-Q_{5510}\left(\frac{\partial^2}{\partial x^2}\phi\right)+4Q_{665}\left(\frac{\partial^4}{\partial x^2\partial y^2}w_s\right)$$
$$+2Q_{124}(\frac{\partial^4}{\partial x^2\partial y^2}w_b)-E_{313}(\frac{\partial^2}{\partial x^2}\phi)=0 \quad (42)$$

$\delta\varphi$:

$$-Q_{5510}\left(\frac{\partial^2}{\partial x^2}w_s\right)-Q_{5510}\left(\frac{\partial^2}{\partial x^2}\phi\right)+E_{1510}\left(\frac{\partial^2}{\partial x^2}\phi\right)$$
$$-Q_{4410}\left(\frac{\partial^2}{\partial y^2}\phi\right)+E_{2410}\left(\frac{\partial^2}{\partial y^2}\phi\right)+\frac{1}{2}K_0\left(\frac{\partial^4}{\partial y^2\partial x^2}\varphi\right)$$
$$+Q_{339}(\varphi)+E_{334}(\phi)+Q_{236}\left(\frac{\partial}{\partial y}v\right)+Q_{136}\left(\frac{\partial}{\partial x}u\right)$$
$$-Q_{137}\left(\frac{\partial^2}{\partial x^2}w_b\right)-Q_{4410}\left(\frac{\partial^2}{\partial y^2}w_s\right)-Q_{237}\left(\frac{\partial^2}{\partial y^2}w_b\right)$$
$$-Q_{238}(\frac{\partial^2}{\partial y^2}w_s)-Q_{138}(\frac{\partial^2}{\partial x^2}w_s)=0 \quad (43)$$

$\delta\phi$:

$$E_{1510}\left(\frac{\partial^2}{\partial x^2}\phi\right)+E_{5510}\left(\frac{\partial^2}{\partial x^2}w_s\right)+D_{111}\left(\frac{\partial^2}{\partial x^2}\phi\right)$$
$$+E_{2410}\left(\frac{\partial^2}{\partial y^2}\phi\right)+E_{2410}\left(\frac{\partial^2}{\partial y^2}w_s\right)+D_{222}\left(\frac{\partial^2}{\partial y^2}\phi\right)$$
$$+E_{320}\left(\frac{\partial}{\partial y}v\right)+E_{310}\left(\frac{\partial}{\partial x}u\right)-E_{311}\left(\frac{\partial^2}{\partial x^2}w_b\right)$$
$$-E_{321}(\frac{\partial^2}{\partial y^2}w_b)-E_{323}(\frac{\partial^2}{\partial y^2}w_s)-E_{313}(\frac{\partial^2}{\partial x^2}w_s)$$
$$+E_{334}\varphi-2D_{331}\phi_0-D_{333}\phi=0 \quad (44)$$

where its coefficients are defined in the Appendix 1.

4. Analytical solution procedure

Navier's technique is selected to solve the governing equations. History of Navier's solution dates back to 1820, when Navier proposed the solution for rectangular simply supported boundary plates as (Khorasani *et al*. 2022, 2021a):

$$u(x,y)=\sum_{m=1}^{M}\sum_{n=1}^{N}U\,sin\{\beta y\}\,cos\{\alpha x\},$$
$$v(x,y)=\sum_{m=1}^{M}\sum_{n=1}^{N}V\,sin\{\alpha x\}\,cos\{\beta y\},$$
$$w_b(x,y)=\sum_{m=1}^{M}\sum_{n=1}^{N}W_b\,sin\{\beta y\}\,sin\{\alpha x\},$$
$$w_s(x,y)=\sum_{m=1}^{M}\sum_{n=1}^{N}W_s\,sin\{\beta y\}\,sin\{\alpha x\},$$
$$\varphi(x,y)=\sum_{m=1}^{M}\sum_{n=1}^{N}\varphi\,sin\{\beta y\}\;sin\{\alpha x\},$$
$$\phi(x,y)=\sum_{m=1}^{M}\sum_{n=1}^{N}\phi\,sin\{\beta y\}\,sin\{\alpha x\} \quad (45)$$

in which $\beta=n\pi/b$ and $\alpha=m\pi/a$. U, V, W_b, W_s, φ and ϕ denote the coefficients which are unknown. (m,n) are mode numbers along (x, y) directions. Finally, the governing equations are introduced as matrix form as:

$$[K]_{6\times6}\begin{bmatrix}U\\V\\W_b\\W_s\\\varphi\\\phi\end{bmatrix}=[0]_{6\times1} \quad (46)$$

The matrix [K] arrays are obtained by mixing Eq. (46) with the governing equations and are presented in Appendix 2.

5. Obtained results explanation

This section addresses the results to provide a clear understanding about the buckling behavior of under-evaluation model. The porous core is made of SUS304 and its properties are visible in Table 2 (Amir *et al*. 2020c). Furthermore, the matrix's properties (Epoxy) and reinforcement's properties (CNTs) as faces' constituents are presented in Table 3 (Han and Elliott 2007).

Moreover, some properties are considered as basic properties which can be presented as:

$$h=0.01m,\qquad h_{t,b,f}=0.1h,\qquad h_c=0.8h,$$
$$a,b=10h,\qquad e_1=0.3,\qquad V_{CNT}=0.17,$$

To verify the presented code and make it reliable, results related to geometrical impacts on dimensionless critical load of buckling is gained by current code and then compared with those of Zhong and Gu (2006), Timoshenko and Gere (1961), and Adhikari *et al*. (2020) in Table 4. The

Table 2 Material properties of the porous core (Amir *et al.* 2020c)

Material	*Properties*	*Value*
SUS304	E_c (Pa)	201.04×10^9
	α_c $(/K)$	12.33×10^{-6}
	ρ_c (kg/m^3)	8166
	v_c	0.3262
	β_c $(/K)$	0.01

Table 3 Material properties of the CNTRCs face sheets (Han and Elliott 2007)

Properties	*SWCNTs*	*PVDF*
N	0.175	0.34
ρ (kg/m^3)	1400	1780
e_{31} (C/m^2)	0	-0.13
e_{32}	0	-0.145
e_{24}	0	-0.276
e_{15}	0	-0.135
$d_{11}=d_{22}=d_{33}$ (Ns/CV)	0	-46
α_{11} $(/K)$	3.4584×10^{-6}	45×10^{-6}
$\alpha_{22}=\alpha_{33}$	5.1682×10^{-6}	
β_{11} $(/K)$	3×10^{-4}	20×10^{-4}
$\beta_{22}=\beta_{33}$	5×10^{-4}	
E_{11} (TPa)	5.6466	E_m (GPa)= 2.2
$E_{22}=E_{33}$	7.0800	
$G_{12}=G_{23}=G_{13}$	1.9445	

Table 4 Comparing the obtained dimensionless critical buckling load for the simply supported isotropic rectangular plate with those of literature for b/h=100

Ref.	*a/b*			
	0.5	1	1.5	2
	Uniaxial loading			
Zhong and Gu (2006)	6.2380	3.9970	4.3370	-
Timoshenko and Gere (1961)	6.2500	4.0000	-	-
Adhikari *et al.* (2020)	6.2418	3.9978	4.3374	3.9981
Present Work	6.2473	4.0001	4.3402	4.0012
	Biaxial loading			
Zhong and Gu (2006)	-	-	-	-
Timoshenko and Gere (1961)	-	-	-	-
Adhikari *et al.* (2020)	4.9935	1.9990	1.4439	1.2496
Present Work	4.9985	2.0009	1.4493	1.2516

nondimensional critical load of buckling in Table 4 is $N^*_{cr}=N_{cr}\frac{b^2}{\pi^2 D},(D=\frac{Eh^3}{12(1-\nu^2)})$. Have a look on Table 4, the results of mentioned papers, include a little bit difference which can be due to the different assumptions or various displacement field using, are the same. So, the current paper's code reliability is guaranteed and its results can provide reliable information about buckling behavior of such light weight structures.

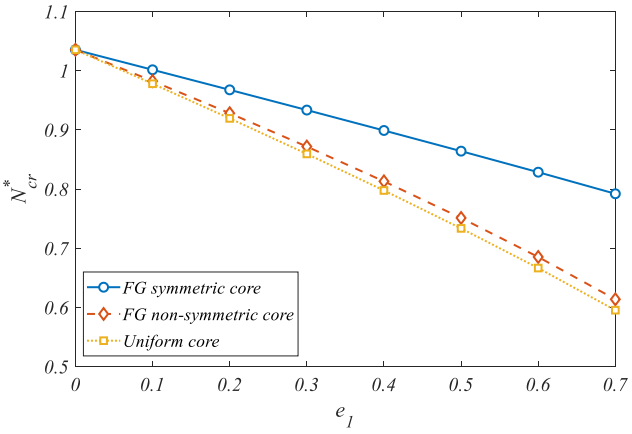

Fig. 2 Effect of porosity coefficient and pores' placement pattern on the dimensionless critical buckling load

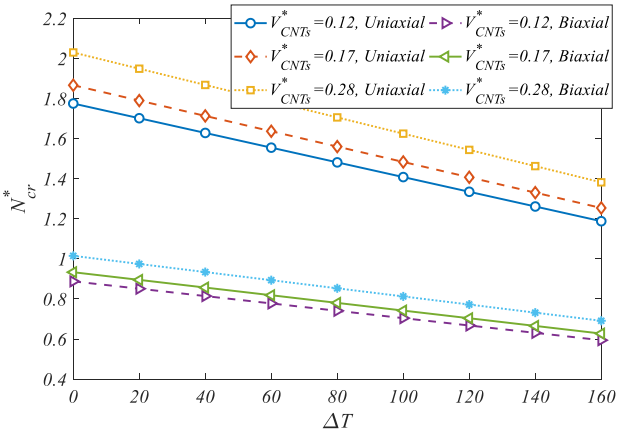

Fig. 3 Effect of CNTs' volume fraction variations in both uniaxial and biaxial loading cases on the results

Now it turns to consider the current work's results. Fig. 2 is presented to study porosity factor effect on the dimensionless critical load of buckling with different types of porosity distribution. As it is evident, symmetric porosity distribution provide higher critical buckling in each porosity coefficient and its effect become more considerable in higher values of porosity coefficients. In order to provide more physical vision toward this figure results, it should be noted that the higher magnitudes of critical buckling mean the higher values of load which is needed to deform under examination sandwich model.

Curvatures plotted in Fig. 3 is responsible to examine the impacts of temperature variations (in Kelvin) and CNTs volume fraction on buckling behavior of model. Relying on the recent figure, CNTs volume fraction and temperature increasing have a vice versa impact on the critical load of buckling and cause more and less load be required to deform model which means higher stiffness and lower stiffness, respectively. Furthermore, by using uniaxial loading more stiff structure can be obtained in comparison with the case of biaxial loading.

Results plotted in Fig. 4 can provide a useful physical vision toward geometrical parameter influences on buckling

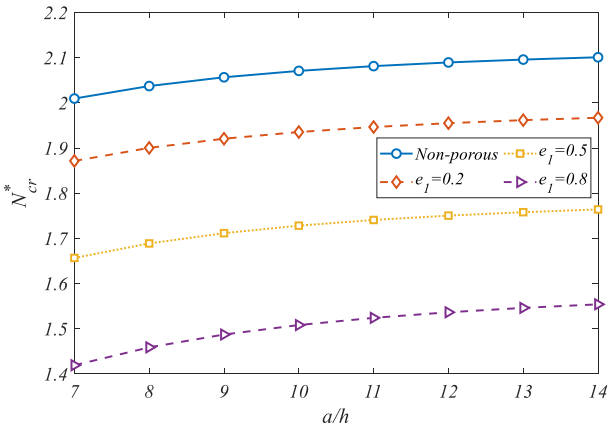

Fig. 4 Effect of porosity and aspect ratio on the dimensionless critical buckling load

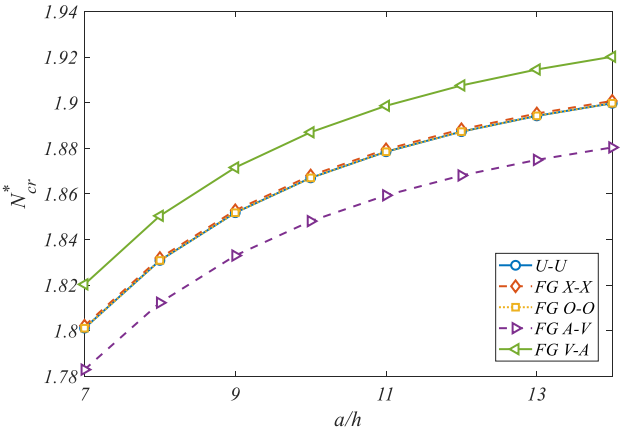

Fig. 6 Influence of CNTs distribution patterns on the critical buckling load of the plate

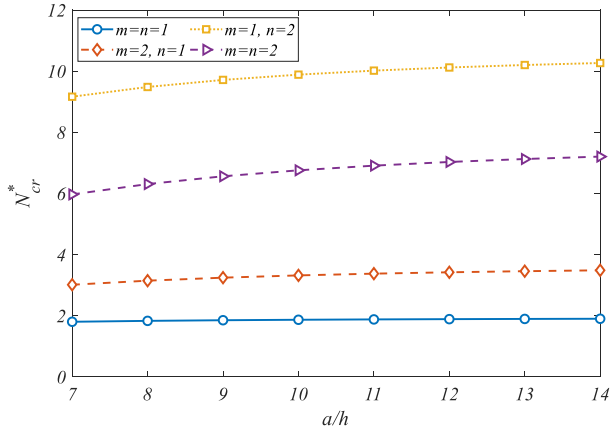

Fig. 5 Different buckling mode numbers

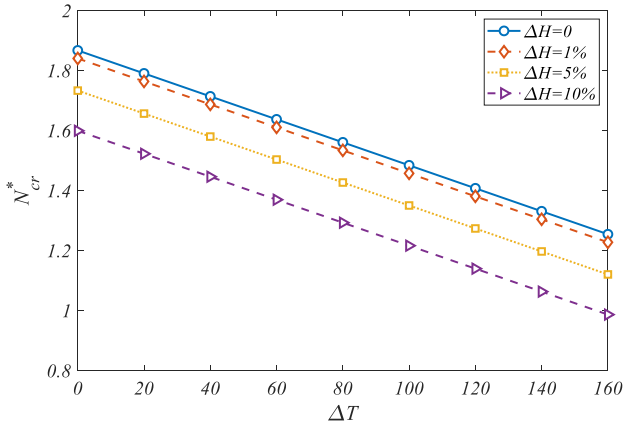

Fig. 7 Temperature and moisture variations effect on the dimensionless critical buckling load

behavior of such light weight models. As it is visible, sandwich structure length to height ratio enhancement results in critical load of buckling enhancement. It should be noted that from aspect ratio equal to twelve on, the response of critical bulking to this ratio variation become more hide. Furthermore, it is revealed that by porosity coefficient enhancement, critical buckling loads and consequently, stiffness reduces dramatically.

Buckling behavior response to mode number variations is plotted in Fig 5. Figure curvatures state that mode number (1,1) provide lowest critical buckling load among other mode numbers. Furthermore, it is proved that mode number (1,2) causes stiffer sandwich structure providing. Fig. 6 shows dimensionless critical buckling load of sandwich structure versus length to thickness ratio for different types of CNTs dispersion pattern. What is interesting in presented figure is that highest and lowest critical buckling load and consequently stiffness, is due to the *V-A* and *A-V* CNTs dispersion type, respectively. However, using *U-U*, *O-O* and *X-X* dispersion pattern of CNT model shows similar stiffness and buckling behavior, meaningful difference between two other CNTs dispersion pattern in critical buckling load can display the importance of dispersing pattern of reinforcing phase in mechanical behavior of current model. Fig. 7 is presented to show the effect of hygrothermal environment on buckling response of such abovementioned structures. As results are plotted in this figure, critical buckling load has a linear dependency to the temperature difference. Increasing temperature difference causes critical buckling load reduction which means less magnitudes of load is needed to deform under-evaluation model. Physical point of view is accessible when have a little bit mindset about material science. As temperature difference increases, molecular bond become softer and less magnitudes of load in needed to change their position which leads to deform structure in simpler way. Furthermore, humidity existence can cause less stiff sandwich structure.

Temperature and porosity changes impact on the critical load of buckling in both uniaxial and biaxial loading cases is investigated in Fig. 8. According to presented figure, it is proved that, porosity coefficient enhancement causes whole structure stiffness reduction. In fact, porosity coefficient is a measure of pores' existence in structure, As mentioned coefficient increases, more porous layer is provided. From physical and practical point of view the range of this coefficient should be between 0 (perfect layer) and 0.99. Porosity coefficient equal to 1 means whole layer is pores and as another expression there is nothing. Fig. 9 is provided to study effect of externally applied voltage on the critical buckling load for different values of length-to-width ratio. As it is clear in mentioned figure, variation of

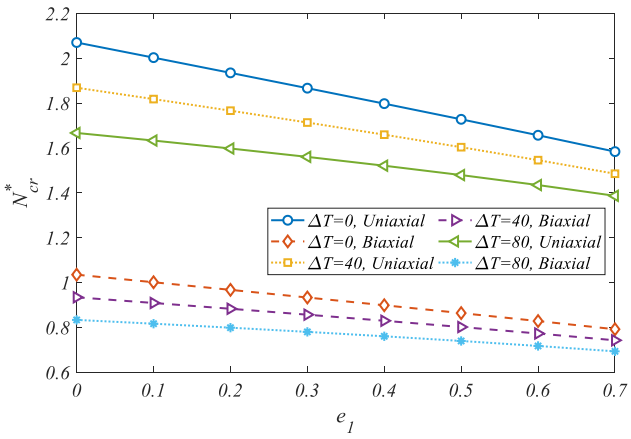

Fig. 8 Porosity and temperature changes effect on the results in both uniaxial and biaxial loading cases

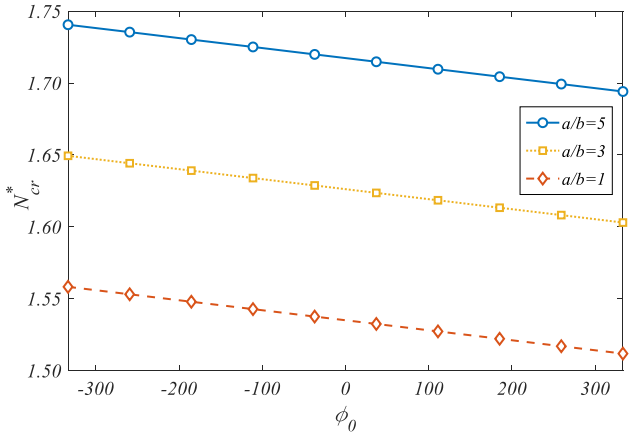

Fig. 9 Effect of externally applied voltage on the critical buckling load

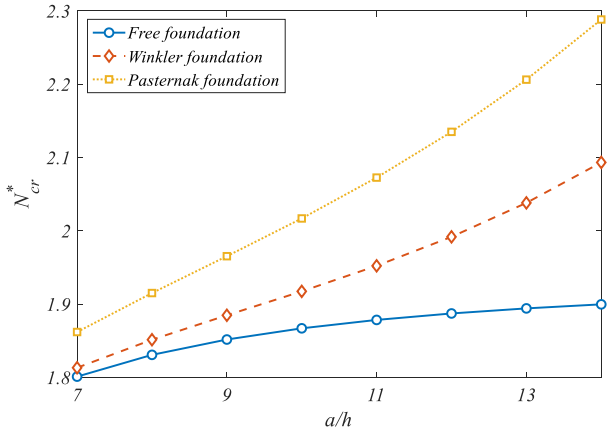

Fig. 10 Comparing effect of different kinds of foundation on the results

electrical voltage in a wide range from -300 to +300 results in critical buckling load reduction linearly. So, it can be concluded that by applying higher magnitudes of negative voltage it is possible to have mechanical behavior improvement which causes stiffness enhancement. Moreover, aspect ratio enhancement results in critical buckling load enhancement.

Finally, Fig. 10 is responsible to compare the effect of different kinds of foundation on the nondimensional critical buckling loads. It is proved that using foundation improve mechanical properties of sandwich structure in each aspect ratio. Also, it is revealed thar Pasternak foundation provide stiffer model in comparison with Winkler and free foundations.

6. Conclusions

A novel QHSDT, and ERM in cooperation with virtual displacement principle are organized to derive governing equations of sandwich model containing FG porous core (SUS304) and FG-CNTRC face sheets to investigate mechanical buckling behavior of mentioned model. It is revealed that increasing the externally applied voltage in negative and positive range cause mechanical behavior enhancement and reduction, respectively. Beside this, as mentioned broadly in previous section, hygrothermal environment existence results in dimensionless critical buckling loads reduction and this behavior are in a good relationship with porosity coefficient enhancement. As another conclusion it is noteworthy mentioning that uniaxial loading in comparison with biaxial loading provide higher values of critical buckling load. To put all in a nut shell, current model analyzation and its results can help to originate more clear and simpler understanding about such light weight structure and presented results hope to be useful for industrial consumption.

Acknowledgment

The fifth author extends his appreciation to the Deanship of Scientific Research at King Khalid University for funding this work through large group Research Project under grant number RGP2/6/44.

References

Adhikari, B., Dash, P. and Singh, B.N. (2020), "Buckling analysis of porous FGM sandwich plates under various types nonuniform edge compression based on higher order shear deformation theory", *Compos. Struct.*, **251**, 112597. https://doi.org/10.1016/j.compstruct.2020.112597.

Alhaifi, K., Arshid, E. and Khorshidvand, A.R. (2021), "Large deflection analysis of functionally graded saturated porous rectangular plates on nonlinear elastic foundation via GDQM", *Steel Compos. Struct.*, **39**(6), 809. https://doi.org/10.12989/SCS.2021.39.6.795.

Alhaifi, K., Khorshidvand, A.R., Al-Masoudy, M.M., Arshid, E. and Madani, S.H. (2023), "A shooting method for buckling and post-buckling analyses of FGSP circular plates considering various patterns of Pores' placement", *Struct. Eng. Mech.*, **85**(3), 432. https://doi.org/10.12989/SEM.2023.85.3.419.

Amir, S., Khorasani, M. and BabaAkbar-Zarei, H. (2018), "Buckling analysis of nanocomposite sandwich plates with piezoelectric face sheets based on flexoelectricity and first-order shear deformation theory", *J. Sandw. Struct. Mater.*, 109963621879538. https://doi.org/10.1177/1099636218795385.

Amir, S., Arshid, E. and Ghorbanpour Arani, M.R. (2019), "Size-dependent magneto-electro-elastic vibration analysis of FG

saturated porous annular/ circular micro sandwich plates embedded with nano-composite face sheets subjected to multi-physical pre loads", *Smart Struct. Syst.*, **23**(5), 429-447. https://doi.org/10.12989/sss.2019.23.5.429.

Amir, S., Arshid, E. and Khoddami Maraghi, Z. (2020a), "Free vibration analysis of magneto-rheological smart annular three-layered plates subjected to magnetic field in viscoelastic medium", *Smart Struct. Syst.*, **25**(5), 581-592. https://doi.org/10.12989/sss.2020.25.5.581.

Amir, S., Arshid, E., Khoddami Maraghi, Z., Loghman, A. and Ghorbanpour Arani, A. (2020b), "Vibration analysis of magnetorheological fluid circular sandwich plates with magnetostrictive facesheets exposed to monotonic magnetic field located on visco-Pasternak substrate", *J. Vib. Control*, **26**(17-18), 1523-1537. https://doi.org/10.1177/1077546319899203.

Amir, S., Arshid, E., Rasti-Alhosseini, S.M.A. and Loghman, A. (2020c), "Quasi-3D tangential shear deformation theory for size-dependent free vibration analysis of three-layered FG porous micro rectangular plate integrated by nano-composite faces in hygrothermal environment", *J. Therm. Stress.*, **43**(2), 133-156. https://doi.org/10.1080/01495739.2019.1660601.

Amir, S., BabaAkbar-Zarei, H. and Khorasani, M. (2020d), "Flexoelectric vibration analysis of nanocomposite sandwich plates", *Mech. Based Des. Struct.*, **48**(2), 146-163. https://doi.org/10.1080/15397734.2019.1624175.

Anh, V.T.T., Huong, V.T., Nguyen, P.D. and Duc, N.D. (2021), "Nonlinear dynamic analysis of porous graphene platelet-reinforced composite sandwich shallow spherical shells", *Mech. Compos. Mater.*, **57**(5), 609-622. https://doi.org/10.1007/S11029-021-09983-W/METRICS.

Arshid, E. and Khorshidvand, A.R. (2018), "Free vibration analysis of saturated porous FG circular plates integrated with piezoelectric actuators via differential quadrature method", *Thin Wall. Struct.*, **125**(January), 220-233. https://doi.org/10.1016/j.tws.2018.01.007.

Arshid, E., Khorshidvand, A.R. and Khorsandijou, S.M. (2019a), "The effect of porosity on free vibration of SPFG circular plates resting on visco-Pasternak elastic foundation based on CPT, FSDT and TSDT", *Struct. Eng. Mech.*, **70**(1), 97-112. https://doi.org/10.12989/sem.2019.70.1.097.

Arshid, E., Kiani, A. and Amir, S. (2019b), "Magneto-electro-elastic vibration of moderately thick FG annular plates subjected to multi physical loads in thermal environment using GDQ method by considering neutral surface", *Mater. Des. Appl.*, **233**(10), 2140-2159. https://doi.org/10.1177/1464420719832626.

Arshid, E., Kiani, A., Amir, S. and Zarghami Dehaghani, M. (2019c), "Asymmetric free vibration analysis of first-order shear deformable functionally graded magneto-electro-thermo-elastic circular plates", *Proceedings of the Institution of Mechanical Engineers, Part C: Journal of Mechanical Engineering Science*, **233**(16), 5659-5675. https://doi.org/10.1177/0954406219850598.

Arshid, E., Amir, S. and Loghman, A. (2020a), "Static and dynamic analyses of FG-GNPs reinforced porous nano-composite annular micro-plates based on MSGT", *Int. J. Mech. Sci.*, **180**(March), 105656. https://doi.org/10.1016/j.ijmecsci.2020.105656.

Arshid, E., Amir, S. and Loghman, A. (2020b), "Bending and buckling behaviors of heterogeneous temperature-dependent micro annular/circular porous sandwich plates integrated by FGPEM nano-Composite layers", *J. Sandw. Struct. Mater.*, 109963622095502. https://doi.org/10.1177/1099636220955027.

Arshid, H., Khorasani, M., Soleimani-Javid, Z., Dimitri, R. and Tornabene, F. (2020c), "Quasi-3D hyperbolic shear deformation theory for the free vibration study of honeycomb microplates with graphene nanoplatelets-reinforced epoxy skins", *Molecules*, **25**(21), 5085. https://doi.org/10.3390/molecules25215085.

Arshid, E. and Amir, S. (2021), "Size-dependent vibration analysis of fluid-infiltrated porous curved microbeams integrated with reinforced functionally graded graphene platelets face sheets considering thickness stretching effect", *Proceedings of the Institution of Mechanical Engineers, Part L: Journal of Materials: Design and Applications*, 146442072098555. https://doi.org/10.1177/1464420720985556.

Arshid, E., Amir, S. and Loghman, A. (2021a), "Thermal buckling analysis of FG graphene nanoplatelets reinforced porous nanocomposite MCST-based annular/circular microplates", *Aerosp. Sci. Technol.*, 106561. https://doi.org/10.1016/j.ast.2021.106561.

Arshid, E., Arshid, H., Amir, S. and Mousavi, S.B. (2021b), "Free vibration and buckling analyses of FG porous sandwich curved microbeams in thermal environment under magnetic field based on modified couple stress theory", *Arch. Civil Mech. Eng.*, **21**(1), 6. https://doi.org/10.1007/s43452-020-00150-x.

Arshid, E., Khorasani, M., Soleimani-Javid, Z., Amir, S. and Tounsi, A. (2021c), "Porosity-dependent vibration analysis of FG microplates embedded by polymeric nanocomposite patches considering hygrothermal effect via an innovative plate theory", *Eng. Comput.*, 1-22. https://doi.org/10.1007/s00366-021-01382-y.

Arshid, E., Soleimani-Javid, Z., Amir, S. and Duc, N.D. (2022), "Higher-order hygro-magneto-electro-thermomechanical analysis of FG-GNPs-reinforced composite cylindrical shells embedded in PEM layers", *Aerosp. Sci. Technol.*, **126**, 107573. https://doi.org/10.1016/J.AST.2022.107573.

Arshid, E., Amir, S. and Loghman, A. (2023a), "Thermoelastic vibration characteristics of asymmetric annular porous reinforced with nano-fillers microplates embedded in an elastic medium: CNTs Vs. GNPs", *Arch. Civil Mech. Eng.*, **23**(2), 100. https://doi.org/10.1007/s43452-023-00624-8.

Arshid, E., Amir, S. and Loghman, A. (2023b), "On the vibrations of FG GNPs-RPN annular plates with piezoelectric/metallic coatings on Kerr elastic substrate considering size dependency and surface stress effects", *Acta Mechanica*, 1-42. https://doi.org/10.1007/S00707-023-03593-4.

Arshid, E., Momeni Nia, M.J., Ghorbani, M.A., Civalek, Ö. and Kumar, A. (2023c), "On the poroelastic vibrations of lightweight FGSP doubly-curved shells integrated with GNPs-reinforced composite coatings in thermal atmospheres", *Appl. Math. Modell.*, **124**, 122-141. https://doi.org/10.1016/j.apm.2023.07.036.

Asgari, G.R., Arabali, A., Babaei, M. and Asemi, K. (2022), "Dynamic instability of sandwich beams made of isotropic core and functionally graded graphene platelets-reinforced composite face sheets", *Int. J. Struct. Stabil. Dyn.*, **22**(8). https://doi.org/10.1142/S0219455422500924.

Babaei, M., Asemi, K. and Safarpour, P. (2019), "Buckling and static analyses of functionally graded saturated porous thick beam resting on elastic foundation based on higher order beam theory", *Iran. J. Mech. Eng. Transact. ISME*, **20**(1), 94-112.

Babaei, M., Hajmohammad, M. H. and Asemi, K. (2020), "Natural frequency and dynamic analyses of functionally graded saturated porous annular sector plate and cylindrical panel based on 3D elasticity", *Aerosp. Sci. Technol.*, **96**, 105524. https://doi.org/10.1016/j.ast.2019.105524.

Babaei, M., Kiarasi, F., Asemi, K., Dimitri, R. and Tornabene, F. (2022a), "Transient thermal stresses in fg porous rotating truncated cones reinforced by graphene platelets", *Appl. Sci.*, **12**(8), 3932. https://doi.org/10.3390/app12083932.

Babaei, M., Kiarasi, F., Asemi, K. and Hosseini, M. (2022b), "Functionally graded saturated porous structures: A review", *J.*

Comput. Appl. Mech., **53**(2), 297-308. https://doi.org/10.22059/JCAMECH.2022.342710.719.

Benahmed, A., Houari, M.S.A., Benyoucef, S., Belakhdar, K. and Tounsi, A. (2017), "A novel quasi-3D hyperbolic shear deformation theory for functionally graded thick rectangular plates on elastic foundation", *Geomech. Eng.*, **12**(1), 9-34. https://doi.org/10.12989/gae.2017.12.1.009.

Berghouti, H., Bedia, E.A.A., Benkhedda, A. and Tounsi, A. (2019), "Vibration analysis of nonlocal porous nanobeams made of functionally graded material", *Adv. Nano Res.*, **7**(5), 351-364. https://doi.org/10.12989/anr.2019.7.5.351.

Bi, R., Gao, J. and Allahyari, S. (2021), "Higher order plate theory for buckling analysis of plates based on exact solution", *Steel Compos. Struct.*, **40**(3), 459. https://doi.org/10.12989/SCS.2021.40.3.451.

Chan, D.Q., Van Thanh, N., Khoa, N.D. and Duc, N.D. (2020), "Nonlinear dynamic analysis of piezoelectric functionally graded porous truncated conical panel in thermal environments", *Thin Wall. Struct.*, **154**, 106837. https://doi.org/10.1016/j.tws.2020.106837.

Cong, P.H., Chien, T.M., Khoa, N.D. and Duc, N.D. (2018), "Nonlinear thermomechanical buckling and post-buckling response of porous FGM plates using Reddy's HSDT", *Aerosp. Sci. Technol.*, **77**, 419-428. https://doi.org/10.1016/j.ast.2018.03.020.

Dat, N.D., Quan, T.Q., Mahesh, V. and Duc, N.D. (2020), "Analytical solutions for nonlinear magneto-electro-elastic vibration of smart sandwich plate with carbon nanotube reinforced nanocomposite core in hygrothermal environment", *Int. J. Mech. Sci.*, **186**, 105906. https://doi.org/10.1016/j.ijmecsci.2020.105906.

Dat, N.D., Quan, T.Q. and Duc, N.D. (2021), "Nonlinear thermal dynamic buckling and global optimization of smart sandwich plate with porous homogeneous core and carbon nanotube reinforced nanocomposite layers", *Eur. J. Mech. A Solids*, **90**, 104351. https://doi.org/10.1016/J.EUROMECHSOL.2021.104351

Dat, N.D., Thanh, N. Van, MinhAnh, V. and Duc, N.D. (2022), "Vibration and nonlinear dynamic analysis of sandwich FG-CNTRC plate with porous core layer", *Mech. Adv. Mater. Struct.*, **29**(10), 1431-1448. https://doi.org/10.1080/15376494.2020.1822476.

Dinh Dat, N., Quoc Quan, T. and Dinh Duc, N. (2022), "Vibration analysis of auxetic laminated plate with magneto-electro-elastic face sheets subjected to blast loading", *Compos. Struct.*, **280**(1), 114925. https://doi.org/10.1016/j.compstruct.2021.114925.

Duc, N.D. (2014), *Nonlinear Static and Dynamic Stability of Functionally Graded Plates and Shells*, Vietnam National University Press, Vietnam.

Duc, N.D., Quang, V.D., Nguyen, P.D. and Chien, T.M. (2018), "Nonlinear dynamic response of functionally graded porous plates on elastic foundation subjected to thermal and mechanical loads", *J. Appl. Comput. Mech.*, **4**(4), 245-259. https://doi.org/10.22055/jacm.2018.23219.1151.

Ebrahimi, F.M.V. (2019), "Vibration analysis of magneto-flexo-electrically actuated porous rotary nanobeams considering thermal effects via nonlocal strain gradient elasticity theory", *Adv. Nano Res.*, **7**(4), 223-231. https://doi.org/10.12989/anr.2019.7.4.223.

Efraim, E. and Eisenberger, M. (2007), "Exact vibration analysis of variable thickness thick annular isotropic and FGM plates", *J. Sound Vib.*, **299**(4-5), 720-738. https://doi.org/10.1016/j.jsv.2006.06.068.

Esfandiari, M., Haghighi, H. and Urgessa, G. (2023), "Machine learning-based optimum reinforced concrete design for progressive collapse", *Electr. J. Struct. Eng.*, **23**(2), 1-8. https://doi.org/10.56748/ejse.233642.

Farhangi, V., Zadehmohamad, M., Monshizadegan, A., Izadifar, M.A., Moradi, M.J. and Dabiri, H. (2023), "Effects of geogrid reinforcement on the backfill of integral bridge abutments", *Buildings*, **13**(4), 853. https://doi.org/10.3390/BUILDINGS13040853.

Fattahi, A.M., Safaei, B. and Moaddab, E. (2019), "The application of nonlocal elasticity to determine vibrational behavior of FG nanoplates", *Steel Compos. Struct.*, **32**(2), 281-292. https://doi.org/10.12989/scs.2019.32.2.281.

Ghorbanpour Arani, A., Rousta Navi, B. and Mohammadimehr, M. (2021), "Buckling and vibration of porous sandwich micro-actuator-microsensor with three-phase carbon nanotubes/fiber/ polymer piezoelectric polymeric nanocomposite face sheets", *Steel Compos. Struct.*, **41**(6), 805-820. https://doi.org/10.12989/SCS.2021.41.6.805.

Guo, H., Zhuang, X. and Rabczuk, T. (2019), "A deep collocation method for the bending analysis of Kirchhoff plate", *Comput. Mater. Continua*, **59**(2), 433-456. https://doi.org/10.32604/cmc.2019.06660.

Han, X., Liu, G.R., Lam, K.Y. and Ohyoshi, T. (2000), "A quadratic layer element for analyzing stress waves in fgms and its application in material characterization", *J. Sound Vib.*, **236**(2), 307-321. https://doi.org/10.1006/jsvi.2000.2966.

Han, X., Liu, G.R. and Lam, K.Y. (2001), "Transient waves in plates of functionally graded materials", *Int. J. Numer. Meth. Eng.*, **52**(8), 851-865. https://doi.org/10.1002/nme.237.

Han, Y. and Elliott, J. (2007), "Molecular dynamics simulations of the elastic properties of polymer/carbon nanotube composites", *Comput. Mater. Sci.*, **39**(2), 315-323. https://doi.org/10.1016/j.commatsci.2006.06.011.

Ikbarieh, A., Izadifar, M. A., Abu-Farsakh, M. Y. and Voyiadjis, G. Z. (2023), "A parametric study of embankment supported by geosynthetic reinforced load transfer platform and timber piles tip on sand", *Transp. Geotech.*, **38**, 100901. https://doi.org/10.1016/J.TRGEO.2022.100901.

Izadifar, M., Mousavi, H., Zadehmohamad, M. and Mir Mohammad Hosseini, S.M. (2021), "Evaluating the isolation effect of the soil-rubber mixture (SRM) around buried pipes during ground vibrations", *7th International Conference on Civil Engineering, Architecture and Urban*. https://doi.org/10.6084/m9.figshare.14998317.

Izadifar, M., Luo, N., Abu-Farsakh, M. Y. and Chen, S. (2023), "Performance evaluation of design methods for geosynthetic-reinforced pile-supported embankments", *Transp. Res. Record: J. Transp. Res. Board*, 036119812311659. https://doi.org/10.1177/03611981231165994.

Javaheri, R. and Eslami, M.R. (2002), "Thermal buckling of functionally graded plates based on higher order theory", *J. Therm. Stress.*, **25**(7), 603-625. https://doi.org/10.1080/01495730290074333.

Kargar, J., Ghorbanpour Arani, A., Arshid, E. and Irani Rahaghi, M. (2021), "Vibration analysis of spherical sandwich panels with MR fluids core and magneto-electro-elastic face sheets resting on orthotropic viscoelastic foundation", *Struct. Eng. Mech.*, **78**(5), 572. https://doi.org/10.12989/SEM.2021.78.5.557.

Khoddami Maraghi, Z., Amir, S. and Arshid, E. (2022), "On the natural frequencies of smart circular plates with magneto-rheological fluid core embedded between magnetostrictive patches on Kerr elastic substance", *Mech. Based Des. Struct.*, 1-18. https://doi.org/10.1080/15397734.2022.2156885.

Khoei, A.R., Youzi, M. and Eshlaghi, G.T. (2022), "Mechanical properties and γ/γ' interfacial misfit network evolution: A study towards the creep behavior of Ni-based single crystal superalloys", *Mech. Mater.*, **171**, 104368. https://doi.org/10.1016/j.mechmat.2022.104368.

Khorasani, M., Eyvazian, A., Karbon, M., Tounsi, A., Lampani, L.,

Sebaey, T.A., Khorasani, M., Eyvazian, A., Karbon, M., Tounsi, A., Lampani, L. and Sebaey, T.A. (2020a), "Magneto-electro-elastic vibration analysis of modified couple stress-based three-layered micro rectangular plates exposed to multi-physical fields considering the flexoelectricity effects", *Smart Struct. Syst.*, **26**(3), 331. https://doi.org/10.12989/SSS.2020.26.3.331.

Khorasani, M., Soleimani-Javid, Z., Arshid, E., Lampani, L. and Civalek, Ö. (2020b), "Thermo-elastic buckling of honeycomb micro plates integrated with FG-GNPs reinforced epoxy skins with stretching effect", *Compos. Struct.*, 113430. https://doi.org/10.1016/j.compstruct.2020.113430.

Khorasani, M., Lampani, L., Dimitri, R. and Tornabene, F. (2021a), "Thermomechanical buckling analysis of the E&amp, P-FGM beams integrated by nanocomposite supports immersed in a hygrothermal environment", *Molecules*, **26**(21), 6594. https://doi.org/10.3390/MOLECULES26216594.

Khorasani, M., Soleimani-Javid, Z., Arshid, E., Amir, S. and Civalek, Ö. (2021b), "Vibration analysis of graphene nano-platelets' reinforced composite plates integrated by piezo-electromagnetic patches on the piezo-electromagnetic media", *Wave. Random Complex Med.*, 1-31. https://doi.org/10.1080/17455030.2021.1956017.

Khorasani, M., Elahi, H., Eugeni, M., Lampani, L. and Civalek, O. (2022), "Vibration of FG porous three-layered beams equipped by agglomerated nanocomposite patches resting on vlasov's foundation", *Transp. Porous Med.*, **142**(1-2), 157-186. https://doi.org/10.1007/S11242-021-01658-3/METRICS.

Kianezhad, M., Youzi, M., Vaezi, M. and Nejat Pishkenari, H. (2022), "Rectilinear motion of carbon nanotube on gold surface", *Int. J. Mech. Sci.*, **217**, 107026. https://doi.org/10.1016/j.ijmecsci.2021.107026.

Kianezhad, M., Youzi, M., Vaezi, M. and Nejat Pishkenari, H. (2023), "Unidirectional motion of C60-based nanovehicles using hybrid substrates with temperature gradient", *Sci. Rep.*, **13**(1), 1100. https://doi.org/10.1038/s41598-023-28245-4.

Kiarasi, F., Babaei, M., Mollaei, S., Mohammadi, M. and Asemi, K. (2021), "Free vibration analysis of FG porous joined truncated conical-cylindrical shell reinforced by graphene platelets", *Adv. Nano Res.*, **11**(4), 380. https://doi.org/10.12989/ANR.2021.11.4.361.

Koizumi, M. (1997), "FGM activities in Japan", *Compos. Part B Eng.*, **28**(1-2), 1-4. https://doi.org/10.1016/s1359-8368(96)00016-9.

Kiarasi, F., Asadi, A., Babaei, M., Asemi, K. and Hosseini, M. (2022), "Dynamic analysis of functionally graded carbon nanotube (FGCNT) reinforced composite beam resting on viscoelastic foundation subjected to impulsive loading", *J. Comput. Appl. Mech.*, **53**(1), 1-23. https://doi.org/10.22059/JCAMECH.2022.339008.693.

Mehar, K. and Panda, S.K. (2017), "Thermal free vibration behavior of fg-cnt reinforced sandwich curved panel using finite element method", *Polym. Compos.*, **39**(8), 2751-2764. https://doi.org/10.1002/pc.

Mehrdad, A., Samadiani, N. and Poormoosa, L. (2013), "Effect of temperature and hydrochloric acid on the intrinsic viscosity of poly(acrylic acid) in aqueous solutions", *J. Mole. Liq.*, **187**, 177-182. https://doi.org/10.1016/j.molliq.2013.06.018.

Mohammadimehr, M., Arshid, E., Alhosseini, S.M.A.R., Amir, S. and Arani, M.R.G. (2019), "Free vibration analysis of thick cylindrical MEE composite shells reinforced CNTs with temperature-dependent properties resting on viscoelastic foundation", *Struct. Eng. Mech.*, **70**(6), 683-702. https://doi.org/10.12989/sem.2019.70.6.683.

Mousavi, S.B., Amir, S., Jafari, A. and Arshid, E. (2021), "Analytical solution for analyzing initial curvature effect on vibrational behavior of PM beams integrated with FGP layers based on trigonometric theories ", *Adv. Nano Res.*, **10**(3), 251. https://doi.org/10.12989/ANR.2021.10.3.235.

Na, K.S. and Kim, J.H. (2003), "Three-dimensional thermal buckling analysis of functionally graded materials", *Compos. Part B Eng.*, **35**(5), 429-437. https://doi.org/10.1016/j.compositesb.2003.11.013.

Najafizadeh, M.M. and Eslami, M.R. (2002), "Buckling analysis of circular plates of functionally graded materials under uniform radial compression", *Int. J. Mech. Sci.*, **44**(12), 2479-2493. http://doi.org/10.1016/S0020-7403(02)00186-8.

Quan, T.Q., Van Quyen, N. and Duc, N.D. (2021), "An analytical approach for nonlinear thermo-electro-elastic forced vibration of piezoelectric penta - Graphene plates", *Eur. J. Mech. A Solids*, **85**, 104095. https://doi.org/10.1016/j.euromechsol.2020.104095.

Quan, T.Q., Anh, V.M., Mahesh, V. and Duc, N.D. (2022a), "Vibration and nonlinear dynamic response of imperfect sandwich piezoelectric auxetic plate", *Mech. Adv. Mater. Struct.*, **29**(1), 127-137. https://doi.org/10.1080/15376494.2020.1752864.

Quan, T.Q., Ha, D.T.T. and Duc, N.D. (2022b), "Analytical solutions for nonlinear vibration of porous functionally graded sandwich plate subjected to blast loading", *Thin Wall. Struct.*, **170**, 108606. https://doi.org/10.1016/j.tws.2021.108606.

Quang, V.D., Khoa, N.D. and Duc, N.D. (2021), "The effect of structural characteristics and external conditions on the dynamic behavior of shear deformable FGM porous plates in thermal environment", *J. Mech. Sci. Technol.*, **35**(8), 3323-3329. https://doi.org/10.1007/S12206-021-0706-X/METRICS.

Rabczuk, T., Ren, H. and Zhuang, X. (2023), *Nonlocal Strong Forms of Thin Plate, Gradient Elasticity, Magneto-Electro-Elasticity and Phase Field Fracture by Nonlocal Operator Method*, Springer International Publishing.

Reddy, J.N. and Chin, C.D. (1998), "Thermomechanical analysis of functionally graded cylinders and plates", *J. Therm. Stress.*, **21**(6), 593-626. https://doi.org/10.1080/01495739808956165.

Safari, M., Mohammadimehr, M. and H. Ashrafi, (2021), "Free vibration of electro-magneto-thermo sandwich Timoshenko beam made of porous core and GPLRC", *Adv. Nano Res.*, **10**(2), 115-128. https://doi.org/10.12989/anr.2021.10.2.115.

Samaniego, E., Anitescu, C., Goswami, S., Nguyen-Thanh, V.M., Guo, H., Hamdia, K., Zhuang, X. and Rabczuk, T. (2020), "An energy approach to the solution of partial differential equations in computational mechanics via machine learning: Concepts, implementation and applications", *Comput. Meth. Appl. Mech. Eng.*, **362**, 112790. https://doi.org/10.1016/j.cma.2019.112790.

Shahsavari, D., Shahsavari, M., Li, L. and Karami, B. (2018), "A novel quasi-3D hyperbolic theory for free vibration of FG plates with porosities resting on Winkler/Pasternak/Kerr foundation", *Aerosp. Sci. Technol.*, **72**, 134-149. https://doi.org/10.1016/j.ast.2017.11.004.

Shen, H.S. (2009), "A comparison of buckling and postbuckling behavior of FGM plates with piezoelectric fiber reinforced composite actuators", *Compos. Struct.*, **91**(3), 375-384. https://doi.org/10.1016/j.compstruct.2009.06.005.

Singh, P.P. and Azam, M.S. (2021), "Size dependent vibration of embedded functionally graded nanoplate in hygrothermal environment by Rayleigh-Ritz method", *Adv. Nano Res.*, **10**(1), 25-42. https://doi.org/10.12989/ANR.2021.10.1.025.

Soleimani-Javid, Z., Arshid, E., Amir, S. and Bodaghi, M. (2021a), "On the higher-order thermal vibrations of FG saturated porous cylindrical micro-shells integrated with nanocomposite skins in viscoelastic medium", *Defence Technol.*, **18**(8), 1416-1434. https://doi.org/10.1016/J.DT.2021.07.007.

Soleimani-Javid, Z., Arshid, E., Khorasani, M., Amir, S. and Tounsi, A. (2021b), "Size-dependent flexoelectricity-based vibration characteristics of honeycomb sandwich plates with various boundary conditions", *Adv. Nano Res.*, **10**(5), 460.

https://doi.org/10.12989/ANR.2021.10.5.449.
Thai, T.Q., Zhuang, X. and Rabczuk, T. (2023), "Curved flexo-electric and piezoelectric micro-beams for nonlinear vibration analysis of energy harvesting", *Int. J. Solids Struct.*, **264**, 112096. https://doi.org/10.1016/J.IJSOLSTR.2022.112096.
Timoshenko, S.P. and Gere, J.M. (1961), *Theory of elastic stability*, McGraw-Hill, New York, U.S.A.
Torabipour, A., Asghari, N., Haghighi, H., Yaghoubi, S. and Urgessa, G. (2023), "Assessing effectiveness of shape memory alloys on the response of bolted T-stub connections subjected to cyclic loading", *CivilEng*, **4**(1), 105-133. https://doi.org/10.3390/civileng4010008.
Vel, S.S., Mewer, R.C. and Batra, R.C. (2004), "Analytical solution for the cylindrical bending vibration of piezoelectric composite plates", *Int. J. Solids Struct.*, **41**(5-6), 1625-1643. https://doi.org/10.1016/j.ijsolstr.2003.10.012.
Vosoughkhosravi, S., Dixon-Grasso, L. and Jafari, A. (2022), "The impact of LEED certification on energy performance and occupant satisfaction: A case study of residential college buildings", *J. Build. Eng.*, **59**, 105097. https://doi.org/10.1016/j.jobe.2022.105097.
Vosoughkhosravi, S. and Jafari, A. (2022a), "Using Wi-Fi position system for developing a privacy-preserving contact tracing system in university campuses", *Comput. Civil Eng.*, 2021, 1236-1244. https://doi.org/10.1061/9780784483893.151.
Vosoughkhosravi, S. and Jafari, A. (2022b), "developing a conceptual passive contact tracing system for commercial buildings using WiFi indoor positioning", *Sustainability*, **14**(16), 10255. https://doi.org/10.3390/su141610255.
Wang, B., Yan, G. and Allahyari, S. (2021), "Optimization and mathematical modelling of multi-layer beam based on sinusoidal theory", *Struct. Eng. Mech.*, **79**(1), 116. https://doi.org/10.12989/SEM.2021.79.1.109.
Wu, Q., Chen, H. and Gao, W. (2020), "Nonlocal strain gradient forced vibrations of FG-GPLRC nanocomposite microbeams", *Eng. Comput.*, **36**(4), 1739-1750. https://doi.org/10.1007/s00366-019-00794-1.
Yang, J., Liew, K.M. and Kitipornchai, S. (2004), "Dynamic stability of laminated FGM plates based on higher-order shear deformation theory", *Comput. Mech.*, **33**(4), 305-315. https://doi.org/10.1007/s00466-003-0533-1.
Zhong, H. and Gu, C. (2006), "Buckling of simply supported rectangular reissner-mindlin plates subjected to linearly varying in-plane loading", *J. Eng. Mech.*, **132**(5), 578-581. https://doi.org/10.1061/(ASCE)0733-9399(2006)132:5(578).
Zhuang, X., Guo, H., Alajlan, N., Zhu, H. and Rabczuk, T. (2021), "Deep autoencoder based energy method for the bending, vibration, and buckling analysis of Kirchhoff plates with transfer learning", *Eur. J. Mech. A Solids*, **87**, 104225. https://doi.org/10.1016/J.EUROMECHSOL.2021.104225

CC

Appendix

The used coefficients in Eqs. (39)-(44) are introduced as below:

$$Q_{110}, Q_{111}, Q_{112} = \int_{h_f} \langle 1, z, z^2 \rangle Q_{11}(z) dz + \int_{h_c} \langle 1, z, z^2 \rangle C_{11}(z) dz,$$

$$Q_{120}, Q_{121}, Q_{122} = \int_{h_f} \langle 1, z, z^2 \rangle Q_{12}(z) dz + \int_{h_c} \langle 1, z, z^2 \rangle C_{12}(z) dz,$$

$$Q_{130}, Q_{131}, Q_{132} = \int_{h_f} \langle 1, z, z^2 \rangle Q_{13}(z) dz + \int_{h_c} \langle 1, z, z^2 \rangle C_{13}(z) dz,$$

$$Q_{230}, Q_{231}, Q_{232} = \int_{h_f} \langle 1, z, z^2 \rangle Q_{23}(z) dz + \int_{h_c} \langle 1, z, z^2 \rangle C_{23}(z) dz,$$

$$Q_{ii0}, Q_{ii1}, Q_{ii2} = \int_{h_f} \langle 1, z, z^2 \rangle Q_{ii}(z) dz + \int_{h_c} \langle 1, z, z^2 \rangle C_{ii}(z) dz, (i = 2, \dots, 6)$$

$$Q_{113}, Q_{114}, Q_{115} = \int_{h_f} \langle 1, z, f(z) \rangle f(z) Q_{11}(z) dz + \int_{h_c} \langle 1, z, f(z) \rangle f(z) C_{11}(z) dz,$$

$$Q_{123}, Q_{124}, Q_{125} = \int_{h_f} \langle 1, z, f(z) \rangle f(z) Q_{12}(z) dz + \int_{h_c} \langle 1, z, f(z) \rangle f(z) C_{12}(z) dz,$$

$$Q_{133}, Q_{134}, Q_{135} = \int_{h_f} \langle 1, z, f(z) \rangle f(z) Q_{13}(z) dz + \int_{h_c} \langle 1, z, f(z) \rangle f(z) C_{13}(z) dz,$$

$$Q_{233}, Q_{234}, Q_{235} = \int_{h_f} \langle 1, z, f(z) \rangle f(z) Q_{23}(z) dz + \int_{h_c} \langle 1, z, f(z) \rangle f(z) C_{23}(z) dz,$$

$$Q_{ii3}, Q_{ii4}, Q_{ii5} = \int_{h_f} \langle 1, z, f(z) \rangle f(z) Q_{ii}(z) dz + \int_{h_c} \langle 1, z, f(z) \rangle f(z) C_{ii}(z) dz, (i = 2,3,4,5,6)$$

$$Q_{116}, Q_{117}, Q_{118} = \int_{h_f} \langle 1, z, f(z) \rangle g'(z) Q_{11}(z) dz + \int_{h_c} \langle 1, z, f(z) \rangle g'(z) C_{11}(z) dz,$$

$$Q_{126}, Q_{127}, Q_{128} = \int_{h_f} \langle 1, z, f(z) \rangle g'(z) Q_{12}(z) dz + \int_{h_c} \langle 1, z, f(z) \rangle g'(z) C_{12}(z) dz,$$

$$Q_{136}, Q_{137}, Q_{138} = \int_{h_f} \langle 1, z, f(z) \rangle g'(z) Q_{13}(z) dz + \int_{h_c} \langle 1, z, f(z) \rangle g'(z) C_{13}(z) dz,$$

$$Q_{236}, Q_{237}, Q_{238} = \int_{h_f} \langle 1, z, f(z) \rangle g'(z) Q_{23}(z) dz + \int_{h_c} \langle 1, z, f(z) \rangle g'(z) C_{23}(z) dz,$$

$$Q_{ii6}, Q_{ii7}, Q_{ii8} = \int_{h_f} \langle 1, z, f(z)\rangle g'(z) Q_{ii}(z) dz + \int_{h_c} \langle 1, z, f(z)\rangle g'(z) C_{ii}(z) dz\,, (i = 2,3,4,5,6)$$

$$Q_{119}, Q_{1110} = \int_{h_f} \langle g'^2(z), g^2(z))\rangle Q_{11}(z) dz + \int_{h_c} \langle g'^2(z), g^2(z))\rangle C_{11}(z) dz,$$

$$Q_{129}, Q_{1210} = \int_{h_f} \langle g'^2(z), g^2(z))\rangle Q_{12}(z) dz + \int_{h_c} \langle g'^2(z), g^2(z))\rangle C_{12}(z) dz,$$

$$Q_{139}, Q_{1310} = \int_{h_f} \langle g'^2(z), g^2(z))\rangle Q_{13}(z) dz + \int_{h_c} \langle g'^2(z), g^2(z))\rangle C_{13}(z) dz,$$

$$Q_{239}, Q_{2310} = \int_{h_f} \langle g'^2(z), g^2(z))\rangle Q_{23}(z) dz + \int_{h_c} \langle g'^2(z), g^2(z))\rangle C_{23}(z) dz,$$

$$Q_{ii9}, Q_{ii10} = \int_{h_f} \langle g'^2(z), g^2(z))\rangle Q_{ii}(z) dz + \int_{h_c} \langle g'^2(z), g^2(z))\rangle C_{ii}(z) dz\,, (i = 2, \ldots, 6)$$

$$E_{310}, E_{311}, E_{313}, E_{314} = \int_{h_f} \langle 1, z, f(z), g'(z)\rangle \frac{\pi}{h_f} sin(\frac{\pi z}{h_f}) e_{31} dz$$

$$E_{320}, E_{321}, E_{323}, E_{324} = \int_{h_f} \langle 1, z, f(z), g'(z)\rangle \frac{\pi}{h_f} sin(\frac{\pi z}{h_f}) e_{32} dz,$$

$$E_{330}, E_{331}, E_{333}, E_{334} = \int_{h_f} \langle 1, z, f(z), g'(z)\rangle \frac{\pi}{h_f} sin(\frac{\pi z}{h_f}) e_{33} dz,$$

$$E_{150}, E_{151}, E_{153}, E_{154} = \int_{h_f} \langle 1, z, f(z), g'(z)\rangle \frac{\pi}{h_f} sin(\frac{\pi z}{h_f}) e_{15} dz,$$

$$E_{240}, E_{241}, E_{243}, E_{244} = \int_{h_f} \langle 1, z, f(z), g'(z)\rangle \frac{\pi}{h_f} sin(\frac{\pi z}{h_f}) e_{24} dz,$$

$$E_{1510}, E_{2410} = \int_{h_f} \langle e_{15}, e_{24}\rangle sin(\frac{\pi z}{h_f}) g(z) dz,$$

$$D_{111}, D_{222} = \int_{h_f} \langle d_{11}, d_{22}\rangle \left[sin(\frac{\pi z}{h_f})\right]^2 dz,$$

$$D_{333}, D_{331} = \int_{h_f} d_{33} \left\langle \left[\frac{\pi}{h_f} sin(\frac{\pi z}{h_f})\right]^2, \frac{\pi}{h^2{}_f} sin(\frac{\pi z}{h_f}) \right\rangle dz$$

Appendix 2

The arrays of matrix [K] can be presented as:

K11	$Q_{110}\alpha^2 + Q_{660}\beta^2$
K12	$Q_{120}\beta\alpha + Q_{660}\beta\alpha$
K13	$-Q_{111}\alpha^3 - Q_{121}\beta^2\alpha - 2Q_{661}\beta^2\alpha$
K14	$-Q_{113}\alpha^3 - Q_{123}\beta^2\alpha - 2Q_{663}\beta^2\alpha$
K15	$-Q_{136}\alpha$
K16	0
K21	$Q_{120}\beta\alpha + Q_{660}\beta\alpha$
K22	$Q_{220}\beta^2 + Q_{660}\alpha^2$
K23	$-Q_{121}\beta\alpha^2 - 2Q_{661}\beta\alpha^2 - Q_{221}\beta^3$
K24	$-Q_{123}\beta\alpha^2 - 2Q_{663}\beta\alpha^2 - Q_{223}\beta^3$
K25	$-Q_{236}\beta$
K26	0
K31	$-Q_{111}\alpha^3 - Q_{121}\beta^2\alpha - 2Q_{661}\beta^2\alpha$
K32	$-Q_{121}\beta\alpha^2 - 2Q_{661}\beta\alpha^2 - Q_{221}\beta^3$
K33	$Q_{112}\alpha^4 + 2Q_{122}\alpha^2\beta^2 + 4Q_{662}\alpha^2\beta^2 + Q_{222}\beta^4$
K34	$Q_{224}\beta^4 + Q_{114}\alpha^4 + 4Q_{664}\alpha^2\beta^2 + 2Q_{124}\alpha^2\beta^2$
K35	$Q_{237}\beta^2 + Q_{137}\alpha^2$
K36	0
K41	$-Q_{113}\alpha^3 - Q_{123}\beta^2\alpha - 2Q_{663}\beta^2\alpha$
K42	$-Q_{123}\beta\alpha^2 - 2Q_{663}\beta\alpha^2 - Q_{223}\beta^3$
K43	$Q_{224}\beta^4 + Q_{114}\alpha^4 + 4Q_{664}\alpha^2\beta^2 + 2Q_{124}\alpha^2\beta^2$
K44	$2Q_{125}\alpha^2\beta^2 + 4Q_{665}\alpha^2\beta^2 + Q_{225}\beta^4 + Q_{115}\alpha^4 + Q_{4410}\beta^2 + Q_{5510}\alpha^2$
K45	$Q_{138}\alpha^2 + Q_{238}\beta^2$
K46	$-E_{1510}\alpha^2 - E_{2410}\beta^2 + Q_{5510}\alpha^2 + Q_{4410}\beta^2$
K51	$-Q_{136}\alpha$
K52	$-Q_{236}\beta$
K53	$Q_{237}\beta^2 + Q_{137}\alpha^2$

K54 $Q_{138}\alpha^2 + Q_{238}\beta^2 + Q_{5510}\alpha^2 + Q_{4410}\beta^2$

K55 Q_{339}

K56 $-E_{1510}\alpha^2 - E_{2410}\beta^2 + Q_{5510}\alpha^2 + Q_{4410}\beta^2$

K61 $-E_{310}\alpha$

K62 $-E_{320}\beta$

K63 $E_{311}\alpha^2 + E_{321}\beta^2$

K64 $-E_{1510}\alpha^2 - E_{2410}\beta^2 + E_{313}\alpha^2 + E_{323}\beta^2$

K65 0

K66 $-E_{1510}\alpha^2 - E_{2410}\beta^2 - D_{111}\alpha^2 - D_{222}\beta^2$